Available online at www.sciencedirect.com
SCIENCE DIRECT®
Journal of Solid State Chemistry 177 (2004) 2339–2349
JOURNAL OF SOLID STATE CHEMISTRY
http://elsevier.com/locate/jssc

Solid solutions of Ni and Co molybdates in silica-dispersed and bulk catalysts prepared by sol–gel and citrate methods

Andrea Maione and Michel Devillers*

Université Catholique de Louvain, Unité de Chimie des Matériaux Inorganiques et Organiques, place Louis Pasteur, 1/3, Louvain-la-Neuve B-1348, Belgium

Received 8 October 2003; received in revised form 9 January 2004; accepted 22 March 2004

Abstract

Silica-dispersed catalysts based on cobalt, nickel and mixed Ni–Co molybdates of various compositions are prepared by a sol–gel procedure from silicon alkoxides, metal nitrates and ammonium heptamolybdate. For comparative purposes, the corresponding bulk molybdates are obtained by the citrate route. The polymorphism and the textural properties of these catalysts are investigated by means of X-ray diffraction, UV–visible diffuse reflectance spectroscopy and Raman spectroscopy. Their surface and textural characteristics are investigated by X-ray photoelectron spectroscopy and nitrogen or krypton physisorption. In the sol–gel prepared catalysts, the β-phase of $Ni_{1-x}Co_xMoO_4$, which is the most active phase in the oxidative dehydrogenation of light alkanes, is stabilized over the whole composition range. In the analogous bulk catalysts prepared by the citrate method, this phase is stabilized only at high Co content ($x \geqslant 0.55$). Dispersion of the active phase in silica is shown to improve the propene productivity in comparison with bulk catalysts obtained by citrate or coprecipitation methods.

Keywords: Nickel molybdate; Cobalt molybdate; Sol–gel; Citrate method; Propane ODH

1. Introduction

Transition metal molybdates are promising catalysts for the oxidative dehydrogenation (ODH) of light alkanes, particularly in the case of propane and isobutane [1–3]. Among all transition metal molybdates, cobalt and nickel molybdates are reported to be the most attractive catalysts. However, they both display a structural polymorphism which makes the interpretation of their catalytic properties quite difficult [4,5]. $NiMoO_4$ may exist in two different phases, noted as α- and β, both of them monoclinic and stable at atmospheric pressure. These phases primarily differ in molybdenum coordination, which is octahedral in the α-phase and tetrahedral in the β-phase [6]. Heating the α-phase up to 948 K generates the pure β-phase, but the latter cannot be quenched at room temperature, because it undergoes the reverse transition on cooling down around 573 K. Mazzocchia et al. [4] studied the catalytic performances of α- and β-$NiMoO_4$, trying to underline the different results they obtained when these phases are tested in propane ODH: both phases display actually a different catalytic activity, the β-phase giving the best results in terms of yield in propene at 833 K.

In a recent work, Dias et al. [7] demonstrated that when SiO_2-supported $NiMoO_4$ is prepared by direct precipitation, β-$NiMoO_4$ is stabilized even at room temperature. Cauzzi et al. [8] applied the sol–gel process via silicon alkoxides in order to allow the formation of β-$NiMoO_4$ dispersed on silica at room temperature. Recently, Zavoianu et al. [9] also showed the possibility to stabilize β-$NiMoO_4$ on TiO_2, by using impregnation or coprecipitation methods. They succeeded in quenching a phase which was so far obtained at room temperature only by using an excess of nickel [10]. Although cobalt molybdate exhibits a similar polymorphism, with α- and β-phases corresponding to the same difference in Mo coordination, its stability scheme is somehow different. Rodriguez et al. [11] investigated the transformation α-$CoMoO_4 \rightarrow \beta$-$CoMoO_4$, which occurs in the temperature range 603–683 K. Upon cooling the obtained β-$CoMoO_4$ to 298 K, there was no formation of the other phase, in contrast with the

*Corresponding author. Fax: +32-10-472-330.
Email-address: devillers@chim.ucl.ac.be (M. Devillers).

0022-4596/$ - see front matter © 2004 Elsevier Inc. All rights reserved.
doi:10.1016/j.jssc.2004.03.022

case of β-$NiMoO_4$. It was therefore concluded that β-$CoMoO_4$ is more stable than β-$NiMoO_4$.

The interest for these compounds is furthermore enhanced by the perspectives of synthesizing mixed Ni–Co molybdates with improved catalytic properties. Stern et al. [12] initiated the investigations on a series of binary nickel–cobalt molybdates displaying improved catalytic properties, whose XRD patterns let conclude that the structures of these mixed compounds are solid solutions of $NiMoO_4$ and $CoMoO_4$ in a common molybdate lattice. Catalytic results on the use of silica-supported $NiMoO_4$ prepared by the sol–gel method, and of silica- or titania-supported $NiMoO_4$, prepared by coprecipitation or impregnation, have been reported in isobutane ODH [7–9]. There were so far no studies on the use of silica-supported Ni–Co molybdates prepared by the sol–gel method in propane ODH.

Considering the undeniable interest of pure Ni and Co molybdates as catalysts for the reactions mentioned above, on one hand, and the fact that their polymorphism and ability to give solid solutions are important parameters in that context, on the other hand, we devoted this work to the synthesis and characterization of mixed Ni–Co molybdates, either as bulk phases or dispersed in a silica matrix. The advantages of the sol–gel procedure will be compared with those of the more classical citrate method [13], in which aqueous solutions of the various metal ions are mixed together in the presence of an excess of citric acid. The materials obtained with these two different preparation methods will be compared from the point of view of their bulk and surface physico-chemical characteristics by means of X-ray diffraction (XRD), Raman spectroscopy, UV–visible diffuse reflectance spectroscopy (UV–vis DRS), surface area and porosity measurements and X-ray photoelectron spectroscopy (XPS). The catalytic behavior of some catalysts was investigated in propane ODH and their performances were compared with those reported for bulk or supported catalysts from the literature, in order to show the importance of dispersing the active phase on a support for this application. Some preliminary results have been presented at international meetings [14,15].

2. Experimental section

2.1. Preparation of Ni–Co molybdates by the citrate method

Adequate amounts of $M(NO_3)_2 \cdot 6H_2O$ (M = Ni and/or Co) (Acros Organics, 99%) and $(NH_4)_6Mo_7O_{24} \cdot 4H_2O$ (Acros Organics, 99%) are dissolved separately in water to obtain the molybdate composition $Ni_{1-x}Co_xMoO_4$ with $x = 0$, 0.25, 0.35, 0.40, 0.45, 0.50, 0.75 and 1.0, and (Ni + Co)/Mo = 1.0. An excess of citric acid (Merck, 99.5%) (1.5 mol citric acid/mol M, M = Ni, Co, Mo) is then added to each solution. The obtained solutions are mixed together and the final solution is concentrated in a rotary evaporator until formation of a viscous liquid, which is then heated at 353 K for 20 h in a vacuum oven. Once a powder has been obtained, the catalyst precursor is pre-calcined at 573 K in a flow of 1 L min^{-1} of dry air, in order to allow the decomposition of the citrate ion involving the formation of CO_2 and water. After the pre-calcination treatment, the catalyst precursor was calcined at 923 K for 20 h in a flow of 1 L min^{-1} of dry air.

2.2. Preparation of silica-dispersed Ni–Co molybdates by the sol–gel method

Adequate amounts of $M(NO_3)_2 \cdot 6H_2O$ (M = Ni and/or Co) and $(NH_4)_6Mo_7O_{24} \cdot 4H_2O$ are dissolved separately in the minimum amount of water in order to obtain final molar ratios corresponding to the following compositions: Ni:Co:Mo $1-x$:x:1 (with $x = 0$, 0.25, 0.50, 0.75 and 1.0). The solutions containing Co and Mo are then added successively dropwise to the Ni solution in order to avoid possible undesired precipitation. Methanol is then added in order to prevent phase separation when TMOS (tetramethoxysilane) (Aldrich, 98%) will be introduced later in the medium (TMOS/CH_3OH = 5/3 vol). The slow addition of TMOS (in amounts corresponding to a Si/Mo molar ratio of 5, 10 or 20) is accompanied by an exothermic reaction. Finally, an aqueous solution of 1 wt% NH_4F (Merck, 95%) (F/Si = 0.01 mol/mol) is added to promote gelation of the catalyst precursor. After gelation, the gels are allowed to age for 3 weeks and then calcined at 773 K (a temperature determined by means of thermogravimetric analysis) during 20 h in a 1 L min^{-1} of dry air flow. For comparative purposes, a sample of pure silica was prepared according to the same experimental procedure, and calcined at 1073 K.

2.3. Instrumental

Thermal analyses have been performed on a Mettler Toledo TGA/SDTA 851 analyzer in an air flow of 100 mL min^{-1} with a temperature increase rate of 10 K min^{-1}.

Powder XRD patterns were measured on a Kristalloflex Siemens D5000 diffractometer using the copper $K\alpha$ radiation ($\lambda = 154.18$ pm). The samples were analyzed after deposition on a quartz monocrystal sample holder supplied by Siemens. The measurements are carried out in 2θ range 10–80° at a scanning rate of 0.01° s^{-1}, the 2θ scale being calibrated with silicon dioxide. The crystalline phases were identified by reference to the powder diffraction data files (JCPDS-ICDD). X-ray thermodiffractometry was performed with the same apparatus, at

an increase rate of $1\,K\,s^{-1}$. The temperature was maintained at 303 K for 10 min before starting the analysis, then XRD patterns were recorded between 673 and 1073 K, after waiting for 1 h at each temperature selected. The temperature was then decreased again to 303 K, at a rate of $10\,K\,s^{-1}$ and a final pattern was recorded at 303 K to check the reversibility of the phase transitions.

XPS was performed on an SSI-X probe (SSX-100/206) spectrometer from FISONS, using the Al$K\alpha$ radiation ($E = 1486.6$ eV) and a ceramic sample holder. Charge compensation was achieved by the use of a flood gun fixed at 8 eV and the use of a nickel grid at 3 mm from the surface of the samples. The energy scale was calibrated by taking the Au $4f_{7/2}$ binding energy at 84 eV. The C 1*s* binding energy of contamination carbon (C–(C–H)) was fixed at 284.8 eV and used as internal standard value. The analyses of nickel, cobalt, oxygen, molybdenum and silicon were based on the following photopeaks: Ni $2p_{3/2}$, Co $2p_{3/2}$, O 1*s*, Mo 3*d* and Si 2*p*. The intensity ratio $I(\text{Mo } 3d_{5/2})/I(\text{Mo } 3d_{3/2})$ was fixed at 1.50 and the difference in binding energy between Mo $3d_{5/2}$ and Mo $3d_{3/2}$ at 3.13 eV.

The BET-specific surface area measurements were carried out on a Micromeritics ASAP 2000 analyzer, using nitrogen or krypton at 77 K. Samples were previously outgassed under vacuum at 473 K. The pore size distribution and total pore volume were determined by using the BJH (desorption) method, assuming a cylindrical pore model.

Raman spectroscopy was performed on a DILOR-JOBIN YVON-SPEX spectrometer, model Olympus DX-40, equipped with a He–Ne ($\lambda = 632.8$ nm) laser.

UV–visible DRS were registered on a UV–vis–NIR spectrometer from Varian, model Cary 5E. The samples have been ground manually on a sample holder and placed in the center of a DRA-C45 integration sphere. Spectra were recorded with background correction in the wavelength range 200–800 nm.

2.4. Catalyst testing

Some catalysts prepared by sol–gel or citrate method were tested in the ODH of propane to propene. The reaction was carried out in a fixed bed U-shaped reactor system working at atmospheric pressure. The experiments were conducted with 250 mg catalyst (particle size 315–200 μm) under the following reaction conditions: volume composition of the reactant mixture: $C_3H_8/O_2/He$:10%:10%:80%; total flow rate $30\,mL\,min^{-1}$, temperature range 673–753 K. The composition of the gaseous mixture at the reactor output was analyzed with a INTERSMAT IGC 12M gas chromatograph, equipped with two 2 m columns, the first one for the separation of propane, propene, CO_2 and water (stationary phase HAYESEP Q), the second one for the analysis of oxygen and the detection of CO (Molecular sieves 5 Å). Usually, carbon monoxide was found to be the only other side product in the catalytic tests. Helium was used as carrier gas and detection was made by catharometry. Successive measurements performed during 1.5 h at constant temperature indicated that the catalytic performances remained unchanged over that period of time. Blank experiments performed in the absence of active phase indicated that in our case, formation of propene via the homogeneous route started at 793 K.

Catalytic results will be expressed as intrinsic propene activity ($\mu mol\,h^{-1}\,m^{-2}$), and propene productivity, expressed as $mmol\,h^{-1}\,g_{ph}^{-1}$ where g_{ph} represents the amount of the active phase dispersed on the support.

3. Results and discussion

3.1. Characterization of Ni, Co and mixed Ni–Co molybdates prepared by the citrate method

3.1.1. Thermal behavior

In the thermograms of almost all citrate gel precursors, a progressive weight loss of 73% is observed between 373 and 873 K. The chemical reactions which are involved in these degradation processes are related to the violent thermal decomposition of the citrate complexes upon oxidation in the presence of oxygen and nitric acid. The standard calcination conditions were fixed at 923 K (i.e., 50 K higher than the final temperature determined by TGA) in a flow of $1\,L\,min^{-1}$ of dry air for 20 h, in order to ensure complete decomposition of the citrate complexes and favor the formation of the crystalline phases.

3.1.2. X-ray diffraction and BET-specific surface areas

Table 1 lists all the citrate-prepared catalysts with their respective BET-specific surface areas and crystalline phases identified by XRD. As indicated, the

Table 1
Composition, specific surface area and crystalline phases detected in pure and mixed Ni–Co molybdates prepared by the citrate method (calcination at 923 K)

Composition	Molar ratio	S_{BET} ($m^2\,g^{-1}$)[a]	Crystalline phases detected
Ni:Mo	1:1	8.3	α-$NiMoO_4$
Co:Mo	1:1	3.1	β-$CoMoO_4$
Ni:Co:Mo	0.75:0.25:1	4.0	α,β-$Ni_{0.75}Co_{0.25}MoO_4$
Ni:Co:Mo	0.50:0.50:1	2.4	α,β-$Ni_{0.50}Co_{0.50}MoO_4$
Ni:Co:Mo	0.45:0.55:1	13.0	β-$Ni_{0.45}Co_{0.55}MoO_4$
Ni:Co:Mo	0.40:0.60:1	5.7	β-$Ni_{0.40}Co_{0.60}MoO_4$
Ni:Co:Mo	0.35:0.65:1	5.4	β-$Ni_{0.35}Co_{0.65}MoO_4$
Ni:Co:Mo	0.25:0.75:1	3.3	β-$Ni_{0.25}Co_{0.75}MoO_4$

[a] Measurements with Kr at 77 K; $\pm 0.02\,m^2\,g^{-1}$.

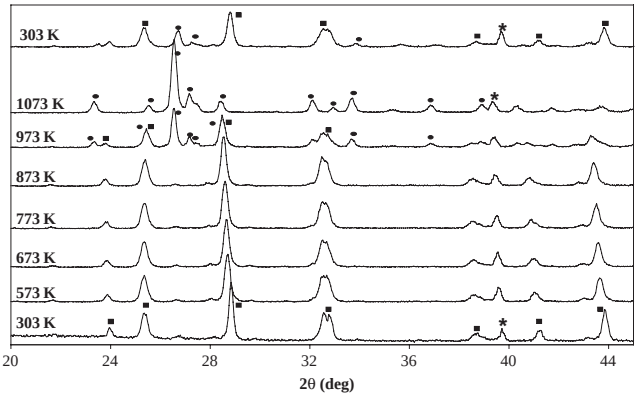

Fig. 1. X-ray thermodiffractometry of $NiMoO_4$ prepared by the citrate method in the temperature range 303–1073 K. (•) β-$NiMoO_4$, (■) α-$NiMoO_4$, and (*) Pt support.

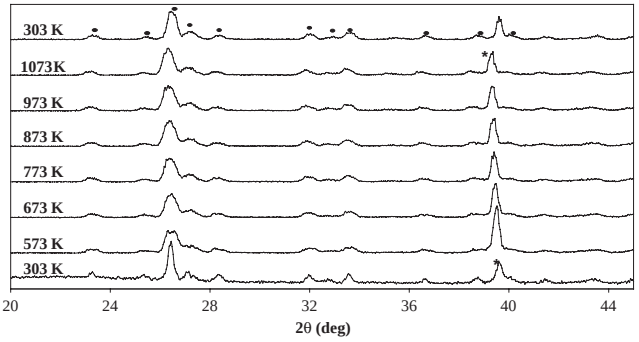

Fig. 2. X-ray thermodiffractometry of $CoMoO_4$ prepared by the citrate method in the temperature range 303–1073 K. (•) β-$CoMoO_4$, and (*) Pt support.

experimental specific surface areas of the mixed Ni–Co molybdates are generally intermediate between those of $NiMoO_4$ and $CoMoO_4$, with the only exception of $Ni_{0.5}Co_{0.5}MoO_4$ and $Ni_{0.45}Co_{0.55}MoO_4$, which exhibit specific surface areas of 2.4 and 13 $m^2\,g^{-1}$, respectively.

In the Ni–Mo–O system, the α-$NiMoO_4$ phase (file 33–0948) with octahedral Mo coordination is identified by XRD through its well-defined pattern displaying peaks at *d*-spacing values of 3.095, 3.513 and 2.746 Å. On the other hand, in the Co–Mo sample, XRD reveals the presence of the β-$CoMoO_4$ phase (file 21–0868) with tetrahedral Mo coordination, evidenced by peaks at *d*-spacing values of 3.360, 3.81 and 3.490 Å. To follow the phase transformations in function of temperature, XRD patterns were also recorded between 303 and 1073 K for both pure $NiMoO_4$ and $CoMoO_4$ samples. They are illustrated in Figs. 1 and 2 for the Ni–Mo and the Co–Mo samples, respectively.

3.1.2.1. $NiMoO_4$. For $NiMoO_4$ (Fig. 1), a phase transformation ($\alpha \rightarrow \beta$) is observed from 973 K, i.e., at a temperature which is about 80 K higher than that reported by Mazzocchia et al. for $NiMoO_4$ prepared by precipitation method [4]. In our case, at 973 K some peaks assigned to the α-phase (file 33–0948) are still present together with those related to the β-phase (file 45–0142), the latter phase being identified through its well-defined XRD pattern with peaks at $2\theta = 23.4°$, 25.6°, 26.6°, 27.2°, 28.5°, 32.1°, 33.7°, the strongest being at 26.6°. At 1073 K, the phase transformation is complete and only the peaks related to the β-phase are observed. When decreasing the temperature from 1073 to 303 K, the opposite transformation ($\beta \rightarrow \alpha$) is observed, even if a small percentage of β-phase still remains. As far as the catalytic applications in propane ODH are concerned, it is important to point out that no phase transformation occurs in the temperature range 673–773 K, which corresponds to the range of usual operation for this reaction.

3.1.2.2. $CoMoO_4$. There are two big differences between the pure Ni and Co molybdates (Fig. 2): first, at room temperature, β-$CoMoO_4$ (file 21–0868) was already identified instead of the α-phase (file 25–1434); second, no phase transformation was observed. The fact that β-$NiMoO_4$, unlike the isotypic $CoMoO_4$ phase, cannot be quenched at ambient temperature is clearly observed.

3.1.2.3. Mixed Ni–Co molybdates. A series of mixed nickel–cobalt molybdates corresponding to the formulation $Ni_{1-x}Co_xMoO_4$ where $x = 0$, 0.25, 0.50, 0.55, 0.60, 0.65, 0.75 and 1, were also prepared by the citrate method.

Fig. 3 displays the XRD pattern of the sample characterized by $x = 0.75$, in which the β-phase is identified through its most intense peaks at $2\theta = 26.5°$(major), 27.1°, 27.45 and 28.4°. As illustrated in Fig. 4, Vegard's law is respected in two different composition domains: the α-phase is detected in the range $0 < x \leqslant 0.5$, while the β-phase is observed in the range $0.25 < x < 1.0$. Fig. 3 also shows that a lattice expansion is observed going from α-$NiMoO_4$ to α-$Ni_{0.5}Co_{0.5}MoO_4$, with a shift in (220) *d*-spacing from 3.092 to 3.109 Å. In the same way, lattice

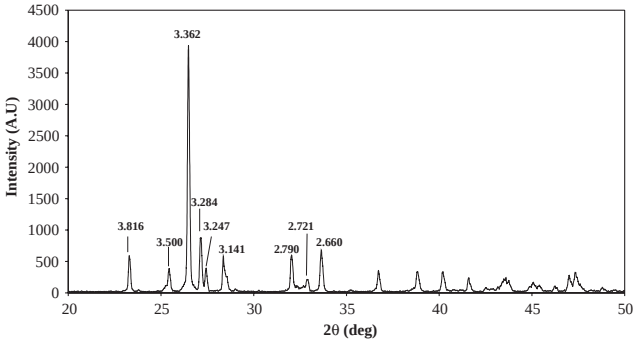

Fig. 3. X-ray diffractrogram of β-$Ni_{0.25}Co_{0.75}MoO_4$ prepared by the citrate method.

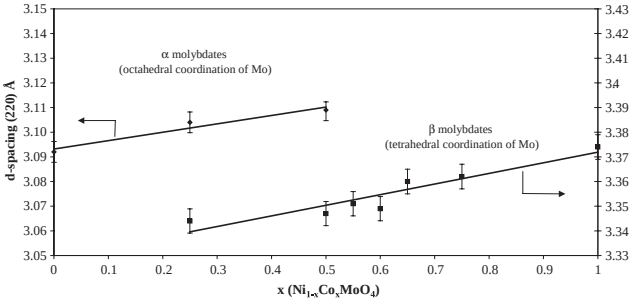

Fig. 4. Verification of Vegard's law with the interreticular (220) d-spacing in $Ni_{1-x}Co_xMoO_4$ prepared by the citrate method. (♦) α-$Ni_{1-x}Co_xMoO_4$, and (■) β-$Ni_{1-x}Co_xMoO_4$.

expansion is observed when going from β-$Ni_{0.75}Co_{0.25}MoO_4$ to β-$CoMoO_4$, as evidenced by the shift in the corresponding d-spacing from 3.344 to 3.374 Å. Only for two intermediate compositions, $x = 0.25$ and 0.5, a mixture of both α and β-phases is detected. It should however be noted that in the case of $CoMoO_4$, the (220) and (002) lines are so close to each other ($d_{2\,2\,0} = 3.362$ Å and $d_{0\,0\,2} = 3.361$ Å) that they overlap. This behavior is consistent with the increase in six coordinate ionic radii of Ni^{2+} (0.69 Å) to Co^{2+} (0.74 Å), which is reflected in the linear increase of d-spacing with the Co/Ni ratio across each region. Since both the cell dimensions and the relative intensities representative of these two compounds vary linearly with Ni/Co atomic ratio, application of Vegard's law [16] led us to conclude that the structures of the mixed nickel–cobalt molybdates in each domain are solid solutions of α-$NiMoO_4$ and α-$CoMoO_4$, on one hand, and of β-$NiMoO_4$ and β-$CoMoO_4$ in a common molybdate lattice, on the other hand.

3.1.3. X-ray photoelectron spectroscopy

In $NiMoO_4$, the experimental atomic ratio (Ni/Mo) is far from the theoretical value corresponding to the bulk composition (0.29 with respect to 1.0); on the other hand, in $CoMoO_4$, the experimental ratio (Co/Mo) agrees quite well with the bulk composition (0.85 for 1.0). In $Ni_{0.5}Co_{0.5}MoO_4$ and $Ni_{0.45}Co_{0.55}MoO_4$, the experimental atomic ratio (Ni + Co/Mo) amounts to 0.6 in both cases, a value which is intermediate between those of M/Mo in pure $NiMoO_4$ and $CoMoO_4$. In these mixed Ni–Co molybdates, the atomic ratio (Ni/Co) is very close to the theoretical value, indicating that the surface Ni–Co composition agrees well with the bulk stoichiometry. On the contrary, the experimental atomic ratios (Ni/Mo) and (Co/Mo) in these two samples differ significantly from the theoretical values (0.26 and 0.37, respectively, instead of 0.45 and 0.55 for $x = 0.55$; 0.30 for both metals instead of 0.50 for $x = 0.5$). The marked differences between the experimental and theoretical M/Mo ratios (M= Ni, Co) for pure $NiMoO_4$ and the solid solutions $Ni_{1-x}Co_xMoO_4$ suggest the presence of MoO_3 at the surface, which was not detectable by XRD nor Raman spectroscopy. It is also interesting to note that, in all citrate-prepared catalysts, the average carbon contamination is in the range of 23–28%, which is quite a lot.

3.1.4. Raman spectroscopy

All the $Ni_{1-x}Co_xMoO_4$ samples have been analyzed by Raman spectroscopy and some illustrative examples are presented in Fig. 5. These data were analyzed by referring to results available in the literature [17–19], and also those obtained with pure phases from this work (Table 2). According to the literature, sampling of α-$NiMoO_4$ is assumed to result in the formation of the so-called α′-phase, which is a distorted form of α-$NiMoO_4$ [17–19], and this has been confirmed in our case. In all other cases, the presence of the β-phase is inferred from the occurrence of two neighbor bands in the range 935–945 cm^{-1}, resulting in a broad band without clear resolution. It should also be pointed out that for the two intermediate compositions in which a mixture of α and β-phases was observed by XRD, the Raman spectra only display bands corresponding to the β-phase.

3.1.5. UV–visible diffuse reflectance spectroscopy

In the Ni–Mo sample, the presence of α-$NiMoO_4$ (detected by XRD) is confirmed by the charge transfer (CT) band occurring below 480 nm, due to the $O^{2-} \rightarrow Mo^{6+}$ CT process, characteristic of octahedrally coordinated Mo [20]. In agreement with previous literature, grinding the Co–Mo sample upon sampling results in a color change from purple to green, suggesting the transformation of β-$CoMoO_4$ (previously detected by XRD) to the α-phase. Fig. 6 displays the UV–vis DR spectrum of $Ni_{0.5}Co_{0.5}MoO_4$; the maxima occurring at 525 and 580 nm are assigned to [CoO_6] octahedra [21]. The fact that only the α-phase is detected while XRD revealed the presence of both α and β-phases in this sample results from the sampling conditions as said above. In all the DR spectra of $Ni_{1-x}Co_xMoO_4$ samples, a CT band starting at 480 nm appears, which is characteristic of the α-phase.

3.2. Characterization of Ni, Co and mixed Ni–Co molybdates prepared by the sol–gel method

3.2.1. Thermal behavior

All sol–gel prepared catalysts are characterized by the same TGA pattern, displaying two successive steps: the first abrupt one, between 373 and 473 K, with a weight loss of 40% is followed by a second one, more progressive, between 473 and 1073 K, with a weight loss of 10%. When comparing with the citrate-prepared catalysts, the total weight loss in the sol–gel compounds is lower (50% vs. 70%). The final temperature at the end of the second degradation step, is also higher (1073 K)

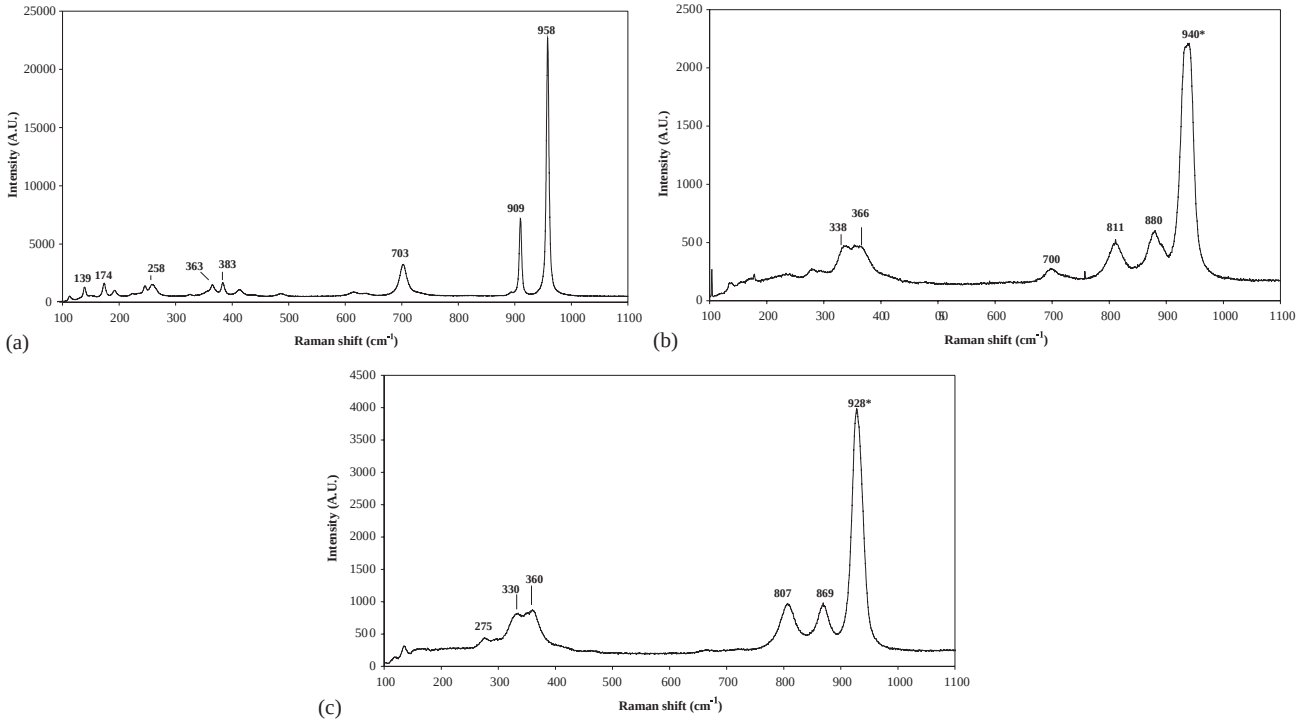

Fig. 5. Raman spectra of (a) α'-$NiMoO_4$, (b) β-$Ni_{0.4}Co_{0.6}MoO_4$, and (c) β-$CoMoO_4$ prepared by the citrate method. The asterisk denotes the presence of a shoulder.

Table 2
Raman data of pure phases prepared by the citrate method and reference data from the literature

Compounds and references	Raman shifts (cm^{-1})
α-$NiMoO_4$ [18]	937, 915, 903, 880, 806, 368, 358, 330
α'-$NiMoO_4$[this work]	958 (vs), 909 (s), 703 (m), 383 (w), 258 (w), 174 (w), 139 (w)
α'-$NiMoO_4$ [17,19]	962 (vs), 914 (s), 706 (m)
β-$NiMoO_4$ [18]	945 (vs), 935 (vs), 896 (s), 884 (m), 823 (s), 365 (s), 330 (s)
α-$CoMoO_4$ [18]	938 (vs), 915 (s), 880 (s), 815 (s), 700 (s), 476 (s), 362 (m), 330 (m)
β-$CoMoO_4$[this work]	928* (vs), 869 (m), 807 (m), 360 (m), 275 (w), 135 (w)
β-$CoMoO_4$ [18]	943 (vs), 935 (vs), 896 (s), 882 (s), 818 (s), 363 (m), 330 (m)
MoO_3 [this work]	994 (vs), 821 (vs), 664 (s), 289 (s), 281 (vs), 155 (s)

* With shoulder.

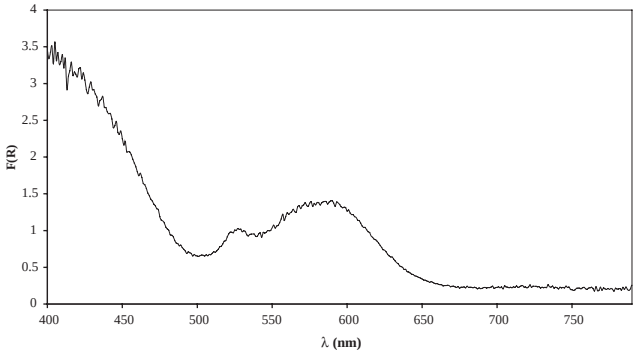

Fig. 6. UV–vis DRS (Kubelka–Munk function) of $Ni_{0.5}Co_{0.5}MoO_4$ prepared by the citrate method.

than in the citrate method (873 K). A standard calcination temperature of 773 K for 20 h under 1 L min^{-1} of dry air flow has been selected for the sol–gel samples.

3.2.2. X-ray diffraction and BET-specific surface areas

Table 3 summarizes the composition of all sol–gel prepared catalysts, their specific surface areas and main crystalline phases identified by XRD. In the Ni–Mo and Co–Mo sol–gel made samples, XRD identifies β-$NiMoO_4$ (file 45–0142) with tetrahedral Mo coordination in the case of $NiMoO_4$ and β-$CoMoO_4$ also in the case of Co–molybdate (file 21–0868). Fig. 7 displays the XRD pattern of a silica-dispersed β-$Ni_{0.5}Co_{0.5}MoO_4$ sample prepared by the sol–gel method. The β-phase is identified through its well-defined XRD pattern with major peaks at $2\theta = 20.8°$, $23.8°$, $25.6°$, $26.6°$(major), $27.4°$ and $28.6°$. In the series of silica-dispersed mixed Ni–Co molybdates, the (220) reflection is common to both structural types and a lattice expansion is observed within the series $Ni_{1-x}Co_xMoO_4$ (Fig. 8), as indicated by the shift in the d-spacing from 3.337 to 3.373 Å (in the samples characterized by Si/Mo = 20), when going from β-$NiMoO_4$ to β-$CoMoO_4$. This behavior is common to all sol–gel samples, independently from the Si content.

Table 3
Composition, specific surface area and crystalline phases detected in pure and mixed Ni–Co molybdates prepared by the sol-–gel method (calcination at 773 K)

Composition	Molar ratio	S_{BET} ($m^2 g^{-1}$)[a]	Detected crystalline phases
Ni:Mo:Si	1:1:20	315	β-$NiMoO_4$
Ni:Mo:Si	1:1:10	288	β-$NiMoO_4$
Ni:Mo:Si	1:1:5	221	β-$NiMoO_4$
Co:Mo:Si	1:1:20	301	β-$CoMoO_4$
Co:Mo:Si	1:1:10	293	β-$CoMoO_4$
Co:Mo:Si	1:1:5	218	β-$CoMoO_4$
Ni:Co:Mo:Si	0.75:0.25:1:20	410	β-$Ni_{0.75}Co_{0.25}MoO_4$
Ni:Co:Mo:Si	0.75:0.25:1:10	317	β-$Ni_{0.75}Co_{0.25}MoO_4$
Ni:Co:Mo:Si	0.75:0.25:1:5	221	β-$Ni_{0.75}Co_{0.25}MoO_4$
Ni:Co:Mo:Si	0.50:0.50:1:20	333	β-$Ni_{0.50}Co_{0.50}MoO_4$
Ni:Co:Mo:Si	0.50:0.50:1:10	296	β-$Ni_{0.50}Co_{0.50}MoO_4$
Ni:Co:Mo:Si	0.50:0.50:1:5	219	β-$Ni_{0.50}Co_{0.50}MoO_4$
Ni:Co:Mo:Si	0.25:0.75:1:20	342	β-$Ni_{0.25}Co_{0.75}MoO_4$
Ni:Co:Mo:Si	0.25:0.75:1:10	298	β-$Ni_{0.25}Co_{0.75}MoO_4$
Ni:Co:Mo:Si	0.25:0.75:1:5	257	β-$Ni_{0.25}Co_{0.75}MoO_4$

[a] Measurement with N_2 at 77 K; $\pm 1\ m^2 g^{-1}$.

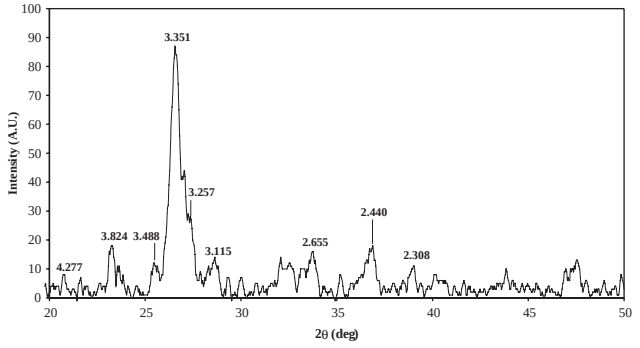

Fig. 7. X-ray diffractrogram of β-$Ni_{0.5}Co_{0.5}MoO_4/SiO_2$ prepared by the sol–gel method (Si/Mo = 5).

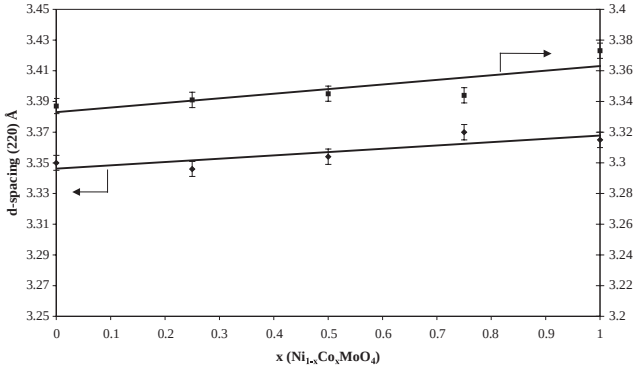

Fig. 8. Verification of Vegard's law with the interreticular (220) *d*-spacing in silica-dispersed β-$Ni_{1-x}Co_xMoO_4$ prepared by the sol–gel method. (♦) Si/Mo = 10, and (■) Si/Mo = 20.

Application of Vegard's law led us to conclude that the structures of these mixed Ni–Co molybdates are again solid solutions of β-$NiMoO_4$ and β-$CoMoO_4$ in a common molybdate lattice.

3.2.3. General comments on specific surface area and porosity measurements

The textural properties of selected SiO_2-supported samples are described in Table 4. These data were determined from complete nitrogen adsorption/desorption isotherms analyzed according to the BET method (for the sample surface area) and to the BJH method (for the pore volume and diameter). All isotherms exhibit the same overall shape corresponding to type IV in Brunauer's classification. Fig. 9 displays an example

Table 4
Textural properties of some silica-dispersed $Ni_{1-x}Co_xMoO_4$ prepared by the sol–gel method

Composition	Molar ratio	S_{BET} ($m^2 g^{-1}$)	V_p ($cm^3 g^{-1}$)[a]	D_p (nm)[b]
Ni:Mo:Si	1:1:20	315	0.70	7.5
Ni:Mo:Si	1:1:10	288	0.44	5.7
Ni:Mo:Si	1:1:5	221	0.53	8.9
Co:Mo:Si	1:1:20	301	0.56	6.5
Co:Mo:Si	1:1:10	293	0.94	11.0
Co:Mo:Si	1:1:5	218	0.67	10.8
Ni:Co:Mo:Si	0.75:0.25:1:20	410	0.54	4.6
Ni:Co:Mo:Si	0.75:0.25:1:10	317	0.75	8.6
Ni:Co:Mo:Si	0.75:0.25:1:5	221	0.52	8.4
Ni:Co:Mo:Si	0.25:0.75:1:20	342	0.79	8.4
Ni:Co:Mo:Si	0.25:0.75:1:10	298	0.55	6.4
Ni:Co:Mo:Si	0.25:0.75:1:5	257	0.80	11.0

The pore size distribution was determined by means of the BJH (desorption) method, assuming a cylindrical pore model.
[a] Average pore volume.
[b] Average pore diameter.

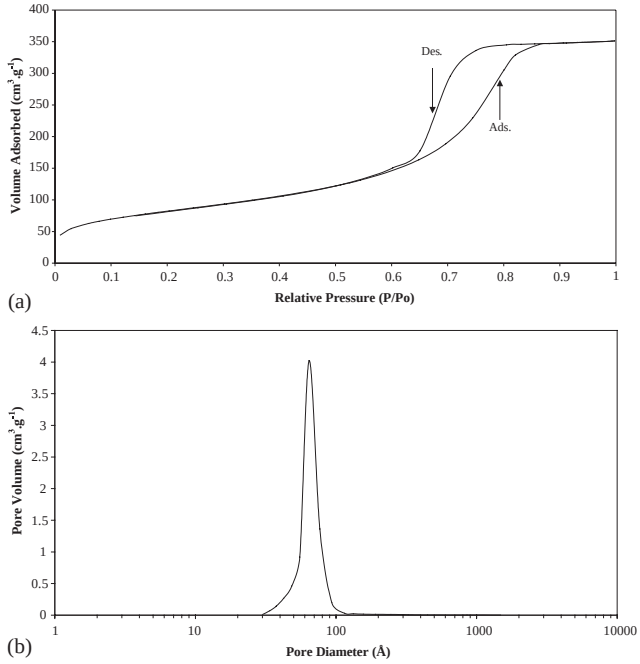

Fig. 9. (a) Nitrogen adsorption–desorption isotherms, and (b) pore distribution from the BJH desorption curve of $Ni_{0.25}Co_{0.75}MoO_4/SiO_2$ (Si/Mo = 10) prepared by the sol–gel method.

of results for the sample with composition $Ni_{0.25}Co_{0.75}MoO_4/SiO_2$ (Si/Mo = 10).

For comparison, the surface characterizations performed on a pure silica sample prepared by the same sol–gel procedure and calcined at 1073 K during 20 h indicated a mesoporous structure with a BET-specific surface area of 215 $m^2 g^{-1}$, an average pore diameter of 5.1 nm (tubular shape) and an average pore volume 0.35 $cm^3 g^{-1}$.

In all SiO_2-dispersed molybdates, the silicon content plays the most important role in the S_{BET} values, the higher the silicon content, the higher the S_{BET} value. The influence of the Ni/Co composition in $Ni_{1-x}Co_xMoO_4/SiO_2$ samples is also well marked: in the catalysts characterized by the (Si/Mo) ratio of 10 or 20, the higher S_{BET} value is observed for $x = 0.25$; for (Si/Mo) = 5, the maximum is observed for $x = 0.75$.

As far as porosity is concerned, in the case of $NiMoO_4$ supported on different amounts of silica, the catalyst with the intermediate molar ratio (Si/Mo) = 10 is characterized by the lowest values of pore volume and pore diameter. The reverse situation is observed for $CoMoO_4$ for which the intermediate loading corresponds to the highest values of pore volume and pore diameter. It thus appears that the dependence of the textural properties is different for the Ni and Co molybdates. As far as the mixed Ni–Co molybdates are concerned, while the Ni–Co–Mo–Si samples characterized by a (Ni/Co) molar ratio of 0.33 display the same behavior as pure $NiMoO_4$, those characterized by (Ni/Co) = 3 exhibit the same behavior as pure $CoMoO_4$. There seems to be only little influence of the Ni/Co composition on the average pore volume and pore size in the catalysts at high loading (Si/Mo = 5); while at lower loading (Si/Mo = 10 or 20), maxima occur but for different compositions.

3.2.4. X-ray photoelectron spectroscopy

Table 5 summarizes the experimental atomic intensity ratios measured by XPS for some sol–gel-prepared catalysts, and the values are compared with the theoretical ones (corresponding to the bulk composition). In both Ni–Mo–Si and Co–Mo–Si samples, the experimental ratios (Ni or Co)/Mo are roughly the same but significantly lower than the corresponding theoretical ones, indicating a substantial enrichment in Mo on the surface. In the same way, the experimental (Ni/Si), (Co/Si) and (Mo/Si) ratios are quite different from those expected from the overall composition. For the pure molybdates, the (Ni/Si) ratios in Ni–Mo–Si-samples are the same as the (Co/Si) ratios in Co–Mo–Si. To evaluate the degree of dispersion of Ni and Co at the surface of mixed molybdate samples, the relative ratios $(M/Si)_{exp}/(M/Si)_{theor}$ (M = Ni, Co) can be calculated from the data listed in Table 5 for $x = 0.75$. The result is found to depend on the silicon content. While Ni and Co are characterized by the same dispersion degree in the sample with the higher silicon content (Si/Mo = 20), reverse situations are observed for the other two compositions: Ni is better dispersed in the sample characterized by Si/Mo = 10, whereas Co is better dispersed than Ni for Si/Mo = 5. The differences between bulk and surface compositions could result from several phenomena: a phase segregation effect related to the preparation or calcination conditions, or partial encapsulation of the active phase in the silica lattice, which is critical from a catalytic point of view because this would restrict the accessibility of these elements.

The binding energies of the various elements were found in the following ranges: 856.7–855.8 eV for Ni $2p_{3/2}$, 781.9–781.0 eV for Co $2p_{3/2}$, 232.5–233.0 eV for Mo $3d_{5/2}$, and 103.5–103.7 eV for Si $2p$, indicating that all these elements appear only with their normally expected oxidation states: Ni(II), Co(II) and Mo(VI). The XPS spectra of oxygen can be resolved into two components corresponding to silica (533 eV) and to the molybdate phase (532 eV), respectively.

Table 5
Relative atomic intensity ratios measured by XPS in the Ni–Co molybdates prepared by the sol–gel method (calcination at 773 K)

Composition and molar ratio	Ni/Mo		Co/Mo		Ni/Co		Ni/Si		Co/Si		Mo/Si	
	Exp	Theor[a]	Exp	Theor[a]	Exp	Theor[a]	Exp	Theor[a]	Exp	Theor[a]	Exp	Theor[a]
Ni:Mo:Si 1:1:20	0.48	1	—	—	—	—	0.007	0.05	—	—	0.016	0.05
Ni:Mo:Si 1:1:10	0.22	1	—	—	—	—	0.006	0.1	—	—	0.027	0.1
Ni:Mo:Si 1:1:5	0.25	1	—	—	—	—	0.012	0.2	—	—	0.051	0.2
Co:Mo:Si 1:1:20	—	—	0.48	1	—	—	—	—	0.007	0.05	0.015	0.05
Co:Mo:Si 1:1:10	—	—	0.21	1	—	—	—	—	0.006	0.1	0.029	0.1
Co:Mo:Si 1:1:5	—	—	0.29	1	—	—	—	—	0.010	0.2	0.035	0.2
Ni:Co:Mo:Si 0.25:0.75:1.20	0.11	0.25	0.36	0.75	0.31	0.33	0.003	0.0125	0.009	0.0375	0.026	0.05
Ni:Co:Mo:Si 0.25:0.75:1.10	0.16	0.25	0.35	0.75	0.46	0.33	0.004	0.025	0.009	0.075	0.026	0.1
Ni:Co:Mo:Si 0.25:0.75:1.5	0.09	0.25	0.43	0.75	0.20	0.33	0.005	0.05	0.026	0.15	0.060	0.2
Ni:Co:Mo:Si 0.5:0.5:1.10	0.28	0.5	0.21	0.5	1.38	1	0.010	0.05	0.007	0.05	0.035	0.1

[a] Values corresponding to the bulk composition.

3.2.5. Raman spectroscopy

All silica-supported $Ni_{1-x}Co_xMoO_4$ samples have been analyzed by Raman spectroscopy and the collected Raman data were compared with those of pure phases (Table 2).

Fig. 10a shows the Raman spectrum of β-$NiMoO_4$, characterized by intense peaks at 955–945, 900 and 827 cm^{-1}, a shape which is very different from that of α'-$NiMoO_4$ obtained by the citrate method (Fig. 5a). Fig. 10c shows the Raman spectrum of β-$CoMoO_4$, with major bands at 925, 869 and 811 cm^{-1}. For the intermediate composition corresponding to β-$Ni_{0.5}Co_{0.5}MoO_4$, (Fig. 10b), the overall shape is similar to those of both simple Ni or Co molybdates, but the most intense band appears at an intermediate value (936 cm^{-1}) when compared with pure β-$NiMoO_4$ and β-$CoMoO_4$. Generally speaking, all Raman spectra of silica-supported $Ni_{1-x}Co_xMoO_4$ display two very close intense bands in the range 940–960 cm^{-1}, leading us to conclude that the Raman data of all Ni–Mo–Si, Co–Mo–Si and Ni–Co–Mo–Si samples are in agreement with the XRD results: the great majority of the bands can be attributed to the β-phase, even if in some cases the presence of MoO_3 is inferred from the line at 990 cm^{-1}.

3.3. Catalytic performances

$NiMoO_4$, $Ni_{0.5}Co_{0.5}MoO_4$ and $Ni_{0.25}Co_{0.75}MoO_4$ prepared by the citrate method were found to display an extremely low catalytic activity in propane ODH, the only product observed being CO_2. This result is obviously due to the very low specific surface areas obtained in that case ($S_{BET} < 13\ m^2\ g^{-1}$).

Table 6 lists the catalytic performances of sol–gel prepared Ni:Co:Mo:Si ($1-x$:x:1:5) catalysts together with some relevant data from the literature. All sol–gel catalysts are characterized by better catalytic performances than the corresponding ones prepared as bulk phases by the citrate method. Dispersion of these molybdates improves therefore definitely their catalytic behavior.

Barsan et al. [22] studied the catalytic performances in propane ODH of β-$Ni_{0.5}Co_{0.5}MoO_4$ prepared by coprecipitation at different pH values. While all those catalysts display a higher intrinsic propene activity (10–60 $\mu mol\ h^{-1}\ m^{-2}$), they show a propene productivity ($\leqslant 2.31\ mmol\ h^{-1}\ g_{ph}^{-1}$) which is two times lower than that of Ni–Co–Mo–Si catalysts prepared by the sol–gel method (5.06 $mmol\ h^{-1}\ g_{ph}^{-1}$). Because the active phase is the same in both cases (β), this is assumed to reflect the advantage of dispersing the active phase in the silica matrix.

The results obtained at 833 K by Stern et al. [12] with silica-supported mixed Ni–Co molybdates prepared by impregnation (80 wt. % of active phase) are also given for comparison. In general, these solid solutions are characterized by lower values of intrinsic propene yield and propene productivity in comparison with simple $NiMoO_4$, while in our case, all solid solutions display

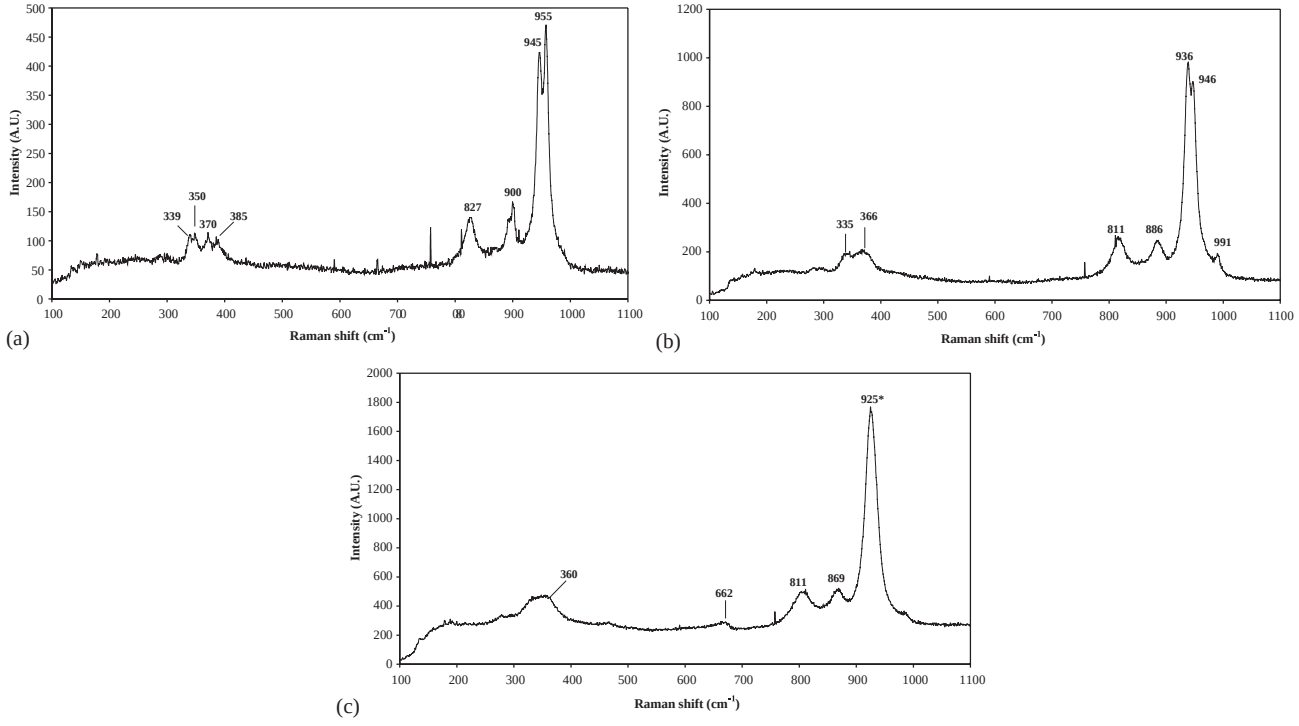

Fig. 10. Raman spectra of (a) β-$NiMoO_4$, (b) β-$Ni_{0.5}Co_{0.5}MoO_4$, and (c) β-$CoMoO_4$ supported on silica (Si/Mo = 5) and prepared by the sol–gel method. The asterisk denotes the presence of a shoulder.

Table 6
Catalytic performances of bulk and silica-dispersed Ni, Co, and Ni–Co molybdate catalysts in propane ODH. Comparison with literature data

Composition and molar ratio	Preparation method	Temperature (K)	Intrinsic propene activity ($\mu mol\,h^{-1}\,m^{-2}$)	Propene productivity ($mmol\,h^{-1}\,g_{ph}^{-1}$)
Ni:Mo:Si 1:1:5	Sol–gel (this work)	753	4.94	2.57
Ni:Co:Mo:Si 0.75:0.25:1:5	Sol–gel (this work)	753	8.69	4.56
Ni:Co:Mo:Si 0.5:0.5:1:5	Sol–gel (this work)	753	10.5	5.06
Ni:Co:Mo:Si 0.25:0.75:1:5	Sol–gel (this work)	753	8.27	4.85
Co:Mo:Si 1:1:5	Sol–gel (this work)	753	6.23	3.23
Ni:Co:Mo 0.5:0.5:1	Coprecip.(pH = 6.0) Ref. [22]	723	58.8	1.35
Ni:Co:Mo 0.5:0.5:1	Coprecip.(pH = 7.5) Ref. [22]	723	11.3	0.68
Ni:Co:Mo 0.5:0.5:1	Coprecip.(pH = 8.5) Ref. [22]	723	22.5	2.31
Ni:Mo:Si 1:1:1.1	Impregnation Ref. [12]	833	124	4.45
Ni:Co:Mo:Si 0.75:0.25:1:1.1	Impregnation Ref. [12]	833	120	3.95
Ni:Co:Mo:Si 0.5:0.5:1:1.1	Impregnation Ref. [12]	833	72.3	2.38
Ni:Co:Mo:Si 0.25:0.75:1:1.1	Impregnation Ref. [12]	833	29.6	0.71
Co:Mo:Si 1:1:1.1	Impregnation Ref. [12]	833	36.1	0.79

better catalytic performances than simple Ni or Co molybdates.

4. Conclusions

The main difference between the bulk and silica-dispersed Ni–Co–Mo catalysts prepared by the citrate or sol–gel methods is related to the fact that it is possible to stabilize the β-$Ni_{1-x}Co_xMoO_4$ phase throughout the whole composition range in the dispersed catalysts, whereas this was not the case at low Co content in the bulk catalysts. This result completes the observations by other authors showing that the pure β-$NiMoO_4$ phase can be stabilized on supports like SiO_2 or TiO_2 when prepared by impregnation or precipitation, or when it is encapsulated in a silica matrix following the sol–gel method [7–9]. According to the literature, the β-phase is normally generated in situ by increasing the temperature to 973 K and could also be stabilized at room temperature in the presence of an excess of Ni. The stabilization of the β-phase at low temperature throughout the Ni–Co composition range, presumably due to interactions between the surface silanol groups and the MoO_4^{2-} species, leading to Si–O–Mo(=O)$_2$–O–Si moieties with tetrahedrally coordinated molybdenum, is therefore very important, because this phase, which is metastable at room temperature, is known to display better catalytic performances in alkane ODH.

The catalytic data emphasize the advantage of using mixed Ni–Co molybdates in comparison with simple Ni or Co molybdates, and also the fact that a higher activity is reached when these active phases are dispersed in a silica matrix, with quite appreciable propene productivities at 753 K. It should also be remembered that the hypothesis of partial encapsulation of the active phase in the silica network was put forward on the basis of the XPS results, and consequently the catalytic behavior of these samples is not yet fully optimized.

Acknowledgments

This work was performed within the frame of a Concerted Research Action of the "Communauté Française de Belgique". The authors also acknowledge the financial support from the Belgian National Fund for Scientific Research (FNRS). They thank Prof. P. Grange (✠) for fruitful discussions and for the access to the XRD, Raman, XPS and catalytic testing equipments. They also thank J.-F. Statsyns, P. Eloy and B. Detienne for their help at various stages of this work.

References

[1] F. Cavani, F. Trifirò, Catal. Today 24 (1995) 307–313.
[2] Y.J. Zhang, I. Rodriguez-Ramos, A. Guerrero-Ruiz, Catal. Today 61 (2000) 377–382.
[3] N.V. Nekrasov, N.A. Gaidai, Y.A. Agafanov, S.L. Kiperman, V. Cortés-Corberán, Stud. Surf. Sci. Catal. B 130 (2000) 1901–1906.
[4] C. Mazzocchia, C. Aboumrad, C. Diagne, E. Tempesti, J.M. Herrmann, G. Thomas, Catal. Lett. 10 (1991) 181–192.
[5] Y.S. Soon, W. Ueda, Y. Moro-oka, Topics Catal. 3 (1996) 265–275.
[6] J.A. Rodriguez, J.C. Hanson, S. Chaturvedi, A. Maiti, J.L. Brito, J. Chem. Phys. 112 (2000) 935–945.
[7] C.R. Dias, R. Zavoianu, M.F. Portela, Catal. Commun. 3 (2002) 85–90.
[8] D. Cauzzi, M. Deltratti, G. Predieri, A. Tiripicchio, A. Kaddouri, C. Mazzocchia, E. Tempesti, A. Armigliato, C. Vignali, Appl. Catal. A: Gen. 182 (1999) 125–135.
[9] R. Zavoianu, C.R. Dias, M.F. Portela, Catal. Commun. 2 (2001) 37–42.
[10] C. Mazzocchia, F. Di Renzo, C. Aboumrad, Solid State Ionics 32/33 (1989) 228–233.
[11] J.A. Rodriguez, S. Chaturvedi, J.C. Hanson, A. Albornoz, J.L. Brito, J. Phys. Chem. B 102 (1998) 1347–1355.
[12] D.L. Stern, R.K. Grasselli, J. Catal. 167 (1997) 550–559.
[13] P. Courty, H. Ajot, C. Marcilly, B. Delmon, Powder Technol. 7 (1973) 21–38.
[14] A. Maione, P. Ruiz, M. Devillers, Extended abstracts of the Fourth World Congress on Oxidation Catalysis, Vol. I, Berlin, Germany, September 2001, pp. 61–64.
[15] A. Maione, P. Ruiz, M. Devillers, Abstracts of the 18th North American Catalysis Society Meeting, Vol. I, p. 284.
[16] A.F. Wells, Structural Inorganic Chemistry, Clarendon Press, Oxford, 1984, p. 1294.
[17] E. Payen, M.C. Dhamelincourt, P. Dhamelincourt, J. Grimblot, J.P. Bonnelle, Appl. Spectrosc. 36 (1982) 30–37.
[18] S. Sheik Salem, Infrared Phys. 27 (1987) 309–315.
[19] M. Woydt, A. Skopp, I. Dorfeland, K. Witke, Wear 218 (1998) 84–95.
[20] S.R.G. Carrazán, C. Martín, V. Rives, R. Vidal, Spectrochim. Acta 52 (1996) 1107–1118.
[21] G.W. Smith, J.A. Ibers, Acta Crystallogr. 19 (1965) 269.
[22] M.M. Barsan, A. Maione, F.C. Thyrion, Stud. Surf. Sci. Catal. 143 (2002) 1063–1072.